

STRESS IN THIN HOLLOW SILICON CYLINDERS GROWN BY THE EDGE-DEFINED FILM-FED GROWTH TECHNIQUE

J.P. KALEJS, A.A. MENNA and R.W. STORMONT

Mobil Solar Energy Corporation, 4 Suburban Park Drive, Billerica, Massachusetts 01821, USA

and

J.W. HUTCHINSON

Division of Applied Sciences, Harvard University, Cambridge, Massachusetts 02138, USA

Received 9 October 1989

Stress behavior is investigated in thin hollow silicon cylinders grown by the edge-defined film-fed growth (EFG) technique. Significant reductions in dislocation density to levels below those typical in ribbon or hollow polygon EFG sheet are observed, but are accompanied by higher residual stresses. A model to predict thermoelastic stresses resulting during growth of a cylinder is presented and the actions of stress components producing creep and residual stress are identified from dislocation and fracture patterns in 15 cm diameter cylinders.

1. Introduction

The edge-defined film-fed growth (EFG) process has been used to produce silicon crystals in the form of ribbons, circular tubes, nine-sided (nonagon) and eight-sided (octagon) closed shape hollow polygons. The widths of the faces of the polygons have progressed up to the current 10 cm of interest in the octagons being evaluated for commercialization [1]. This trend has demonstrated the need for a model to predict stresses that must go beyond that proposed for plane sheets [2]. The hollow thin cylinder provides a starting point for study of stress in the more complicated polygon geometry. It represents a limiting case geometrically for when the polygon diameter increases and the ratio of face width to diameter decreases. The axisymmetric geometry of the cylinder reduces the number of stress components acting on the sheet, when placed in a non-uniform temperature field typical of that needed for high speed growth, to only those acting through the sheet thickness. This provides a unique opportunity to study the manifestations of the

stresses that lead to fracture and to creep in a situation that is considerably simplified over that found in the polygon geometry.

The growth of cylinders of 1 and 8 cm in diameter by EFG has been described previously [3]. The following section presents the experimental work carried out to characterize the stress manifestations in EFG cylinders 15 cm in diameter. The results of fracture and defect studies are given in section 3. An analytical model that allows calculation of thermoelastic stresses on a cylinder resulting from steady-state growth in an arbitrary temperature field is presented in section 4 and used to help interpret the experimental manifestations of the stress.

2. Experimental details

Thin hollow cylinders of 15 cm diameter and 100 to 400 μm thicknesses were grown by the EFG technique from a furnace configuration normally used for production of nonagons [4], with only the die changed to a circular geometry. Pull-

ing rates were 1.5 to 2.5 cm/min for the material examined in this study. Residual stresses were estimated from material deformation after scribing and fracturing sections of the cylinder, while dislocation densities were obtained from examination of cross sectional micrographs.

3. Results

Estimates of the material residual stress may be deduced from an examination of deformation behavior after scribing and fracturing of grown cylinders. The two principal fracture patterns observed are illustrated in fig. 1. Fig. 1a shows a section of the cylinder with an axial fracture that is the predominant mode of failure observed in thicker cylinders (above about 400 μm in thickness). In fig. 1b, the fracture results in crack propagation in a horizontal direction, or transverse to the growth axis of the cylinder. This mode was observed to dominate in the thinner cylinders, below about 200 μm in thickness.

Estimates of the residual stress producing the material deformations were obtained in two ways. The gap arising from a longitudinal cut, as illustrated in fig. 1a, provides information on the azimuthal component of stress $\sigma_{\theta\theta}$ (see fig. 3 for

coordinate specification). Out-of-plane deflections of strips of the cylinder cut along the axial direction are proportional to the axial stress component σ_{xx} . In the latter case, these strips need to be cut to be very narrow so as to minimize the effect of cylinder curvature normal to its axis in order to obtain good estimates. Both of these stress components act through the thickness of the sheet and produce bending modes that are common to cylinders and hollow polygons. However, the main axial in-plane principal stresses studied in plane sheets [2] are absent in the cylindrical geometry because of symmetry.

The bending stress responsible for producing the deformation in fig. 1a, $\sigma_{\theta\theta}$, is a factor of two to three lower than σ_{xx} , so here we neglect contributions of this type to changes in curvature and discuss only means to estimate the latter from experimental observations. In this situation, the maximum value, σ_{xx}^0 , of the fiber stress component σ_{xx} at the surface is approximately given by the expression

$$\sigma_{xx}^0 \cong -\frac{Et \Delta\kappa}{2(1-\nu^2)}. \quad (1)$$

This assumes that the stress varies linearly through the thickness, and it is compressive on the inside and tensile on the outside cylinder surface. Values

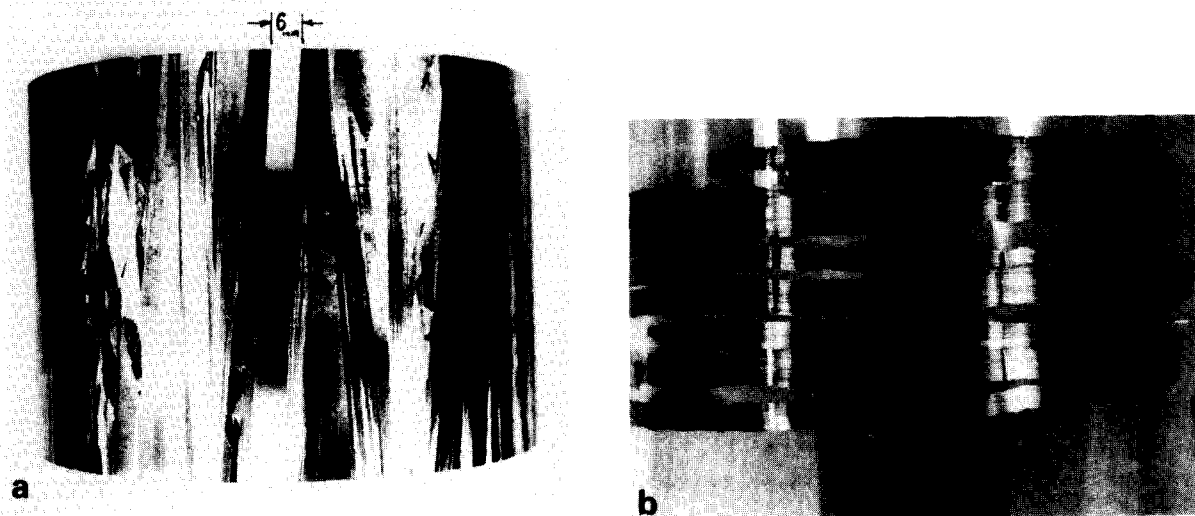


Fig. 1. (a) EFG cylinder section showing fracture pattern produced by $\sigma_{\theta\theta}$ stress in opening up a gap of 6 mm in 15 cm diameter cylinder. The section has been etched in NaOH at 80 $^{\circ}\text{C}$. (b) Spiral fracture in EFG cylinder produced by σ_{xx} .

for the elastic modulus E and for the Poisson ratio ν of 165 GPa and 0.3, respectively, were used in the calculations. The material thickness is t , and $\Delta\kappa$ is the change in curvature of the strip, which may be approximated by $2\delta x/l^2$ for an out-of-plane deflection δx of a strip of length l . The values of σ_{xx} calculated from measured δx for the cylinders using this expression ranged from 15 to 50 MPa. This stress was very inhomogeneous, indicating nonuniform stress relaxation due to creep. Stress variations as large as a factor of two were observed for adjacent strips of a few mm in width. The magnitude of this stress is considerably greater than the bending stresses observed in individual faces of ribbons or polygons (nonagons or octagons), which are typically in the range from 5 to 10 MPa. Peak in-plane residual stresses of this order also were measured in ribbons and in nonagons using shadow moiré interferometry [5], and these exhibited a level of inhomogeneity similar to that found here for the bending stresses.

The defects observed in the cylinders in cross section are similar to those in ribbons and hollow

polygons – dislocations and twins, but dislocation densities are generally a factor of 5 to 10 lower. Regions of very high dislocation density ($\geq 10^7/\text{cm}^3$) and shear bands attributed to Lüders instabilities are observed much less frequently in cylinders than in ribbon grown under known high stress conditions [6]. The typical grain structure is revealed by etching in NaOH, as in fig. 1a. Dislocation patterns that are of relevance in the study of stress here are shown in fig. 2. These were more common in the thinner material, at thicknesses below about 200 μm . Fig. 2a shows a region of very uniform dislocation density extending through the entire thickness of the sample. The pattern in the longitudinal cross section in fig. 2b was observed in material lightly doped with aluminum. Here the dislocations appear in rows along (111) slip planes that originate on the outside surface of the cylinder, but extend only part of the way through the thickness. This leaves a significant region near the inside cylinder surface dislocation-free. The reduced defect density was reflected in the as-grown material quality. Minority carrier

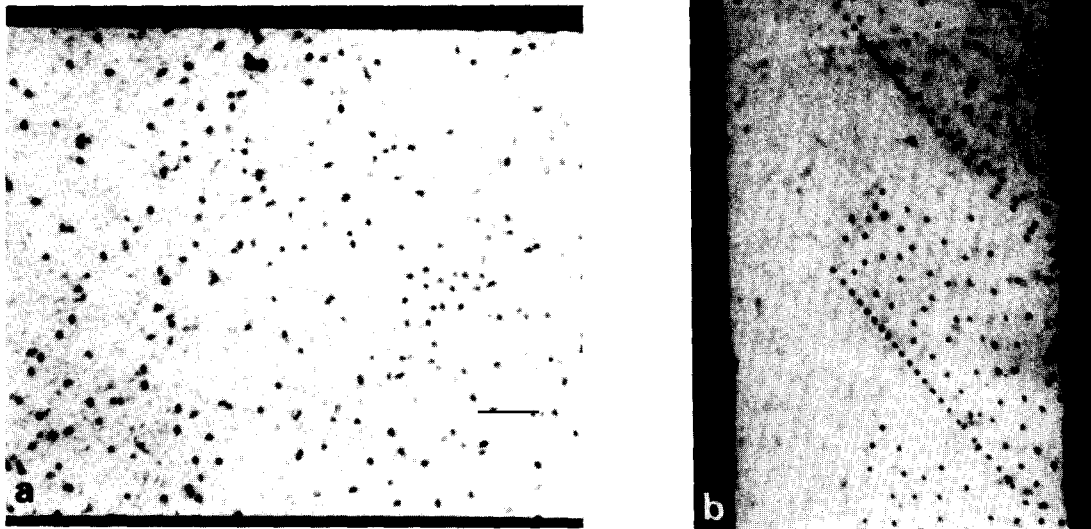


Fig. 2. (a) Cross sectional micrographs of EFG cylinder grown at 2.3 cm/min taken normal to growth direction. Cylinder thickness is 125 μm with a dislocation density of about $8 \times 10^5/\text{cm}^3$. (b) Cross sectional micrograph of 100 μm thick EFG cylinder grown at 2.0 cm/min taken along growth axis. Cylinder inside surface is at left.

diffusion lengths in the range of 60 to 100 μm were in excess of those observed in ribbon or closed shape polygons.

4. Stress model

The symmetry of a closed shape cylindrical geometry makes it possible to obtain exact analytical expressions for the thermoelastic stress distribution imposed on a cylinder subjected to a temperature field. We distinguish here the situation when an initially stress-free cylinder is placed in a temperature field from that for a cylinder in steady-state growth. In the latter case, which best represents the crystal growth situation, we use first order axisymmetric shell theory to derive the maximum stresses acting on the cylinder, which occur at room temperature for a monotonically decreasing temperature profile typical of many sheet growth systems. These results are discussed below.

The (x, θ) coordinate system and variables used to represent growth of a cylinder of thickness t and radius R at a speed V are depicted in fig. 3. The melt interface is placed at $x = 0$ and a zero-stress condition is imposed on the cylinder there;

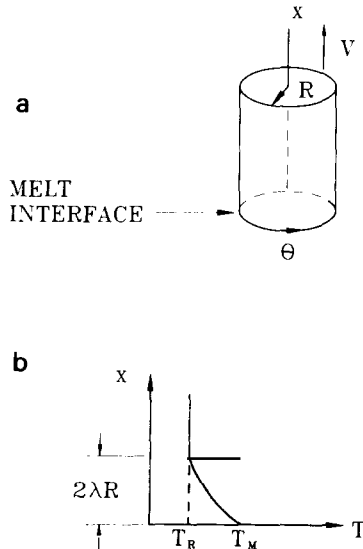


Fig. 3. Notation used for stress model of cylinder: (a) growth and (b) temperature field variables.

z is the coordinate through the thickness (range $-t \leq z \leq t$). The cylinder is subjected to a temperature profile that extends from the melting point T_M to room temperature T_R with an exponential spatial variation:

$$T(x) = \Delta T \exp\left(-\frac{x}{\lambda R}\right) + T_R, \quad (3)$$

with

$$\lambda = \frac{\Delta T}{R} \left[-\left(\frac{\partial T}{\partial x}\right)_0 \right]^{-1}.$$

$\Delta T = T_M - T_R$ and λ is a nondimensional coordinate such that $2\lambda R$ is the characteristic length over which T_M decreases to T_R . λ is also related to the interface temperature gradient $(\partial T/\partial x)_0$ as shown. The stresses at room temperature ($x \rightarrow \infty$) are of primary interest, and these may be written as follows under assumptions of a linear distribution through the thickness arising from the bending:

$$\sigma_{xx}(z) = \sigma_{xx}^0 \left(\frac{z}{\frac{1}{2}t}\right), \quad \sigma_{\theta\theta}(z) = \nu \sigma_{xx}(z), \quad (4)$$

with the outer fiber stress

$$\sigma_{xx}^0 = \frac{E\alpha \Delta T}{2(1-\nu^2)} \frac{t}{R} \frac{1}{\lambda^2} f(q),$$

$$f(q) = \left(1 + \frac{1}{q^4}\right)^{-1} \left[\left(1 - \frac{1}{q^2}\right)^2 + \frac{2 - \sqrt{2}}{q} \right],$$

$$q = [12(1-\nu^2)(R/t)^2]^{1/4} \lambda.$$

The function $f(q)$ is given in fig. 4. A value of $\alpha = 2.55 \times 10^{-6}$ per degree that is independent of temperature is assumed for the thermal expansion coefficient for the purposes of the discussion of these stresses here.

The magnitudes of the stresses of eq. (4) depend critically on the specification of λ . A normal cooling profile for the EFG process is such that the sheet cools from T_M to room temperature over a distance of about 15 cm. Then $2\lambda R \approx 15$ cm, and $\lambda \approx 1$ for the cylinders with $R = 7.5$ cm under consideration. $f(q)$ in eq. (4) is also of the order of unity, and this leads to predictions of unrealistically low stresses, less than about 1 MPa for

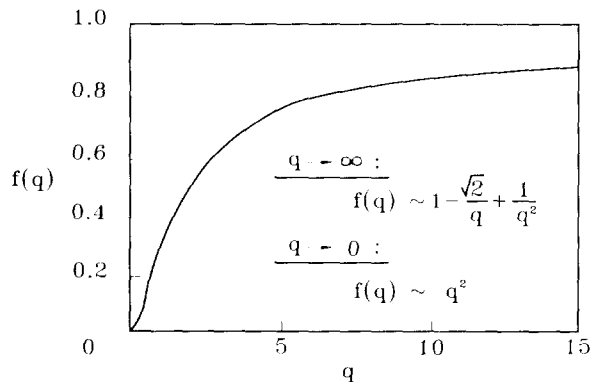


Fig. 4. Functional dependence of $f(q)$, defined in the text, used for calculating thermoelastic stress components from eq. (4).

sheet thicknesses in the range of 100–400 μm . Peak thermoelastic stresses must be several orders of magnitude greater than this to be able to induce a level of creep that would be sufficient to lead to the residual stresses of 15–50 MPa measured experimentally. This requires that λ be about 0.1 and $2\lambda R \approx 1.5$ cm; for a 100 μm thick sheet, $q \approx 5$, $f \approx 0.75$ and with $\Delta T = 1400^\circ\text{C}$, $\sigma_{xx} \approx 32$ MPa. This value of $2\lambda R$ now is significantly shorter than the distance over which the sheet cools to room temperature in the furnace. The implication is that it represents the distance over which creep is acting to produce the dislocations contributing to the observed residual stress, because interface-region solid gradients are sufficiently steep such that this could take place within 2 cm of the interface. By this time the sheet has cooled to the temperature range 1100–1200 $^\circ\text{C}$ and perhaps is work-hardened to the point where subsequent plastic deformation contributes very little to the final residual stress level. If this view is adopted, then we must use a value of ΔT in the range of 200 to 300 $^\circ\text{C}$ and identify T_R with the temperature for which the plastic region terminates. A detailed calculation of residual stresses needs to incorporate the effects of creep, which is beyond the scope of this model.

The fracture and dislocation manifestations detailed in section 3 give insight into other limits of validity of the thermoelastic stress model. The dislocation distribution that is in evidence in fig.

2b would be expected to arise from σ_{xx} , which is tensile on the outside surface of the cylinder and compressive on the inside. As noted above, fractures of the orientation shown in fig. 1b may also be attributed to σ_{xx} , while the axial fracture in fig. 1a requires $\sigma_{\theta\theta}$ to be dominant. The evidence that the former contributes predominantly to relaxation and residual stress in thinner sheet and the latter in the thicker sheet is an indication of changes in the nature of the stress relaxation as thickness decreases: the contribution of $\sigma_{\theta\theta}$ to creep and to residual stress decreases relative to that from σ_{xx} . This behavior is outside of the scope of the thermoelastic stress model in which $\sigma_{\theta\theta}$ is constrained to remain always less than σ_{xx} .

5. Conclusions

Stress manifestations have been studied in thin hollow silicon cylinders grown by the EFG technique. Dislocation densities are lower than in ribbon or closed shaped polygon (nonagons and octagons) EFG material grown with comparable (although not identical) temperature profiles. However, residual stresses are higher. The behavior of stress components was examined using fracture behavior and dislocation patterns, and compared to a thermoelastic stress model for the cylindrical geometry. Evidence is found for the action of stress components through the sheet thickness only, as predicted by the model. The presence of residual stresses greater than those found in ribbons and closed shape polygons is not understood. These were expected to be reduced in the cylinders below those in the polygons because the axisymmetric geometry eliminates large in-plane stresses. The creep response of the sheet during growth is likely responsible for these differences, and a model for the cylinder that includes plastic deformation is required to obtain a better understanding of these effects.

References

- [1] D.S. Harvey, J. Crystal Growth 104 (1990) 88.
- [2] J.C. Lambropoulos, J.W. Hutchinson, R.O. Bell, B. Chalmers and J.P. Kalejs, J. Crystal Growth 65 (1983) 324.

- [3] L. Eriss, R.W. Stormont, T. Surek and A.S. Taylor, *J. Crystal Growth* 50 (1980) 200;
A.S. Taylor, R.W. Stormont, C.C. Chao and E.J. Henderson, in: *Proc. 15th IEEE Photovoltaic Specialists Conf.*, Orlando, FL (IEEE, New York, 1981) p. 589.
- [4] A.S. Taylor, B.H. Mackintosh, L. Eriss and F.V. Wald, *J. Crystal Growth* 82 (1987) 134.
- [5] Y. Kwon, S. Danyluk, L. Bucciarelli and J.P. Kalejs, *J. Crystal Growth* 82 (1987) 221.
- [6] J.P. Kalejs, in: *Silicon Processing for Photovoltaics II*, Eds. C.P. Khattak and K.V. Ravi (Elsevier, Amsterdam, 1987) ch. 4.